Stress Compensation Method for Shakedown Analysis and Its Engineering Applications

Heng Peng, Yinghua Liu, and Haofeng Chen

Abstract This paper introduces a recently proposed direct method, the so-called stress compensation method (SCM), for shakedown analysis of engineering structures under variable repeated mechanical and thermal loads. Instead of establishing the mathematical programming formulation, the SCM performs a two-level iterative procedure based on a series of linear finite element (FE) solutions. By adding an extra stress (named the compensation stress) to the yield regions which may occur at every load vertex of the given loading domain to adjust the total stress to the yield surface and re-solving the equilibrium equations, the residual stress field for static shakedown analysis is constructed. An effective and robust iteration control scheme is presented to check the change of the compensation stress in the inner loop and to update the shakedown load multiplier in the outer loop. The numerical scheme of this method is successfully implemented into the Abaqus platform, which makes it become a general utility tool for shakedown analysis of complex structures. Numerous examples related to pressure vessel and power plant engineering are presented to illustrate the performance of the method for shakedown analysis of large-scale engineering structures under multi-dimensional loading domain.

Keywords Direct method · Shakedown · Stress compensation method · Cyclic loading

H. Peng · Y. Liu (✉)
Department of Engineering Mechanics, AML, Tsinghua University, Beijing 100084, China
e-mail: yhliu@mail.tsinghua.edu.cn

H. Peng
e-mail: pengheng17@mails.tsinghua.edu.cn

H. Chen
Department of Mechanical and Aerospace Engineering, University of Strathclyde, Glasgow G1 1XJ, UK
e-mail: haofeng.chen@strath.ac.uk

A. A. Pisano et al. (eds.), *Direct Methods*, Lecture Notes in Applied and Computational Mechanics 95, https://doi.org/10.1007/978-3-030-48834-5_8

1 Introduction

In the fields of petrochemical industry, nuclear energy, civil engineering and power plant engineering, many structural components made of ductile metals operate under cyclic loadings. Locally, these components may exhibit material plastic yielding during operation. In this case, it is rather conservative to adopt the traditional elastic analysis design. On the contrary, the limit and shakedown analysis makes use of the plasticity of materials, and therefore reflects the nature of bearing capacity and the actual safety margin of structures. Design methods considering the limit and shakedown analysis are now becoming increasingly popular in practical engineering applications [1].

The shakedown analysis aims to determine the load-bearing capacity of structural components under the action of cyclic loadings, so that these components will not fail due to the instantaneous collapse, incremental collapse or alternating plasticity. As is known that, there are two methods of evaluating the shakedown limit [2]: step-by-step (SBS) incremental procedures and direct method.

In the SBS method, a sequence of cyclic steady calculations at different loading levels are performed, and meanwhile, the loads are adjusted to approach to the shakedown limit using the trial-and-error procedures [2]. However, these time stepping calculation processes are often cumbersome and time-consuming, because every load cycle may include many increments and it usually takes a number of load cycles to compute the response of structure to be stable. Furthermore, the shakedown limit calculated may be inaccurate because of the ambiguous stopping conditions and the accumulative errors in numerical calculations.

In the direct method, the shakedown limit is calculated directly using the shakedown theory, with no needing to perform these cumbersome time stepping calculations. In addition, only the bounding envelope rather than the detailed history of applied loads is required. Most of the direct methods transform the shakedown analysis into a special mathematical programming problem, which contains many equal and unequal restriction conditions. Many optimization methods, such as the second order cone programming [3], the sequential quadratic programming, the complex method [4], the interior point method (IPM) [5, 6], and the nonlinear Newton-type iteration algorithms [7–9], are widely applied for solving the shakedown problems. However, the mesh discretization of finite element (FE) analysis produces a great deal of degrees of freedom, which will generate a large-scale mathematical programming problem, especially when a practical engineering structure is considered. Except for the mathematical programming methods, some other numerical direct methods have been developed which avoid the difficulties of direct optimization, including the elastic compensation method [10, 11], the linear matching method [12–14], the residual stress decomposition method [15, 16], and the stress compensation method (SCM) [17, 18]. Up to now, it is still a challenge and important topic to develop efficient and reliable computational methods so that the limit and shakedown theories can display well their applications in engineering practice and solve broader practical problems.

As one of direct methods recently proposed, the SCM presents good computational advantages in solving the shakedown problem of elastic-perfectly plastic (EPP) material under multiple thermomechanical loadings, especially for large-scale complex engineering structures. In this paper, the authors introduce the SCM from the fundamental theory, the numerical procedure, and its applications to practical engineering structures in the fields of pressure vessel and power plant engineering.

2 SCM for Shakedown Analysis

2.1 Melan's Static Shakedown Theorem

For a body of volume V, the stress $\boldsymbol{\sigma}(\mathbf{x}, t)$ of a point $\mathbf{x}$ at the instant t can be decomposed into a fictitious elastic stress $\boldsymbol{\sigma}^E(\mathbf{x}, t)$ and a residual stress $\boldsymbol{\rho}(\mathbf{x}, t)$, i.e.

$$\boldsymbol{\sigma}(\mathbf{x}, t) = \boldsymbol{\sigma}^E(\mathbf{x}, t) + \boldsymbol{\rho}(\mathbf{x}, t) \tag{1}$$

where $\boldsymbol{\sigma}^E(\mathbf{x}, t)$ is the stress solution of an elastic body with the same geometry and load conditions as the body.

If a structure is subjected to multiple loads $\mathbf{P}_i(\mathbf{x}, t)$, $i = 1, 2, \ldots, N$, where each load $\mathbf{P}_i(\mathbf{x}, t)$ is decided by a time-dependent loading parameter $\mu_i(t)$ and a base load $\mathbf{P}_i^0(\mathbf{x})$. The loading history $\mathbf{P}(\mathbf{x}, t)$ can be expressed as

$$\mathbf{P}(\mathbf{x}, t) = \sum_{i=1}^{N} \mathbf{P}_i(\mathbf{x}, t) = \sum_{i=1}^{N} \mu_i(t)\mathbf{P}_i^0(\mathbf{x}) \tag{2}$$

Referring to Eq. (2), the fictitious elastic stress $\boldsymbol{\sigma}^E(\mathbf{x}, t)$ is expressed as

$$\boldsymbol{\sigma}^E(\mathbf{x}, t) = \sum_{i=1}^{N} \boldsymbol{\sigma}_i(\mathbf{x}, t) = \sum_{i=1}^{N} \mu_i(t)\boldsymbol{\sigma}_i^0(\mathbf{x}) \tag{3}$$

where $\boldsymbol{\sigma}_i^0(\mathbf{x})$ is the elastic stress for the base load $\mathbf{P}_i^0(\mathbf{x})$.

The static shakedown theorem is stated as follows: a body will shake down, if there exists a time-independent residual stress field $\boldsymbol{\rho}(\mathbf{x})$, such that its superposition with the fictitious elastic stress field $\lambda \cdot \boldsymbol{\sigma}^E(\mathbf{x}, t)$, resulting in a stress state $\boldsymbol{\sigma}(\mathbf{x}, t)$, does not violate the yield condition at every material point [19].

$$\boldsymbol{\sigma}(\mathbf{x}, t) = \lambda \cdot \boldsymbol{\sigma}^E(\mathbf{x}, t) + \boldsymbol{\rho}(\mathbf{x}) \tag{4}$$

$$\begin{aligned} f = F(\boldsymbol{\sigma}(\mathbf{x}, t)) - \sigma_y(\theta) \le 0 \qquad & \forall \mathbf{x} \in V, \forall t \\ \nabla \cdot \boldsymbol{\rho}(\mathbf{x}) = 0 \qquad & \text{in } V \\ \boldsymbol{\rho}(\mathbf{x}) \cdot \mathbf{n} = 0 \qquad & \text{on } S_t \end{aligned} \tag{5}$$

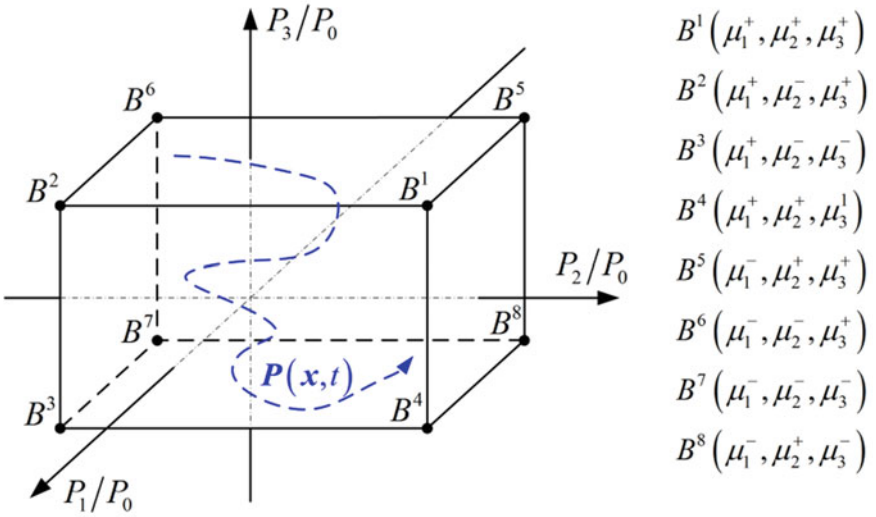

Fig. 1 A polyhedron of eight vertices in 3D loading space [21]

where λ is the load multiplier; f is the yield function; $\sigma_y(\theta)$ is the temperature-dependent yield stress corresponding to temperature θ; $\nabla\cdot$ is the divergence operator; and $\mathbf{n}$ is the unit outward normal to the surface S_t . It is worth noting that the yield function f is required to be convex in $\sigma - \theta$ space [20]. After each update of the load multiplier, the yield stress is also calculated and updated.

It is noted that in most situations the loading parameters $\mu_i(t)$ are not known but only their bounds. If the bounds of each loading parameter are as follows:

$$\mu_i^- \le \mu_i(t) \le \mu_i^+ \tag{6}$$

the bounding envelope of applied loads is determined, which is a polyhedron of $NV = 2^N$ vertices. Figure 1 displays a polyhedron of eight vertices (B^1, B^2, B^3, B^4, B^5, B^6, B^7 and B^8) in three-dimensional (3D) loading space when three loads varying independently within their own limits are considered [21].

The theorem proposed by König indicates that, if a body shakes down over a specific load path traversing all vertices of a polyhedron, then it shakes down over any load path contained within the bounding envelope [2]. Therefore, the shakedown conditions are only tested on these load vertices.

2.2 Description of the SCM

The total strain rate $\dot{\boldsymbol{\varepsilon}}(t)$ contains the elastic strain rate $\dot{\boldsymbol{\varepsilon}}^E(t)$, thermal strain rate $\dot{\boldsymbol{\varepsilon}}_\theta(t)$, plastic strain rate $\dot{\boldsymbol{\varepsilon}}^p(t)$, and residual elastic strain rate $\dot{\boldsymbol{\varepsilon}}_r^e(t)$, i.e.

$$\dot{\boldsymbol{\varepsilon}}(t) = \lambda\left[\dot{\boldsymbol{\varepsilon}}^{E}(t) + \dot{\boldsymbol{\varepsilon}}_{\theta}(t)\right] + \dot{\boldsymbol{\varepsilon}}^{p}(t) + \dot{\boldsymbol{\varepsilon}}_{r}^{e}(t) \tag{7}$$

Making use of the principle of virtual work, the FE global equilibrium equation is established as

$$\left(\int_{V} \mathbf{B}^{T} \cdot \mathbf{D} \cdot \mathbf{B} dV\right) \cdot \dot{\mathbf{u}}(t) = \lambda \int_{V} \mathbf{B}^{T} \cdot \mathbf{D} \cdot \left[\dot{\boldsymbol{\varepsilon}}^{E}(t) + \dot{\boldsymbol{\varepsilon}}_{\theta}(t)\right] dV + \int_{V} \mathbf{B}^{T} \cdot \mathbf{D} \cdot \dot{\boldsymbol{\varepsilon}}^{p}(t) dV \tag{8}$$

Here $\mathbf{D} \cdot \dot{\boldsymbol{\varepsilon}}^{p}(t)$ is replaced by the compensation stress $\boldsymbol{\sigma}^{C}(t)$, which is calculated by

$$\boldsymbol{\sigma}^{C}(t) = \xi(t) \cdot \boldsymbol{\sigma}(t), \xi(t) = \begin{cases} \frac{\bar{\sigma}(t) - \sigma_{y}(\theta)}{\bar{\sigma}(t)} & \left(\bar{\sigma}(t) > \sigma_{y}(\theta)\right) \\ 0 & \left(\bar{\sigma}(t) \le \sigma_{y}(\theta)\right) \end{cases} \tag{9}$$

where $\bar{\sigma}(t)$ is the equivalent stress. Then Eq. (8) is written as

$$\mathbf{K} \cdot \dot{\mathbf{u}}(t) = \lambda \int_{V} \mathbf{B}^{T} \cdot \dot{\boldsymbol{\sigma}}^{E}(t) dV + \lambda \int_{V} \mathbf{B}^{T} \cdot \mathbf{D} \cdot \dot{\boldsymbol{\varepsilon}}_{\theta}(t) dV + \int_{V} \mathbf{B}^{T} \cdot \boldsymbol{\sigma}^{C}(t) dV$$
$$\text{where } \mathbf{K} = \int_{V} \mathbf{B}^{T} \cdot \mathbf{D} \cdot \mathbf{B} dV \tag{10}$$

The residual stress field for static shakedown is obtained by

$$\dot{\boldsymbol{\rho}}(t) = \mathbf{D} \cdot \mathbf{B} \cdot \dot{\mathbf{u}}(t) - \lambda \dot{\boldsymbol{\sigma}}^{E}(t) - \lambda \mathbf{D} \cdot \dot{\boldsymbol{\varepsilon}}_{\theta}(t) - \boldsymbol{\sigma}^{C}(t) \tag{11}$$

$$\boldsymbol{\rho}(t + \Delta t) = \boldsymbol{\rho}(t) + \int_{t}^{t+\Delta t} \dot{\boldsymbol{\rho}}(t) dt \tag{12}$$

The SCM for shakedown analysis consists of two iteration loops. The numerical implementation is as follows:

(1) Calculate the fictitious stress field for each base load, initialize the residual stress field $\boldsymbol{\rho} = 0$, and set an initial load multiplier λ^{ini} . Enter the outer loop where the number of iterations is marked as k.
(2) Enter the inner loop where the number of iterations is marked as m. For each load vertex i, calculate the total stress at every Gauss point.

$$\boldsymbol{\sigma}(t_i) = \lambda^{(k)} \boldsymbol{\sigma}^{E}(t_i) + \boldsymbol{\rho}(t_i) \tag{13}$$

(3) Calculate the compensation stress $\boldsymbol{\sigma}^{C}(t_i)$ and the dimensionless parameter ξ using Eq. (9).
(4) After traversing all the load vertices, the residual stress $\boldsymbol{\rho}_{0}^{(m+1)}$ is updated by Eqs. (14)–(16).

$$\mathbf{K}\cdot\Delta\mathbf{u}=\sum_{i=1}^{NV}\left\{\lambda^{(k)}\int_V\mathbf{B}^T\cdot\left[\Delta\boldsymbol{\sigma}^E(t_i)+\mathbf{D}\cdot\Delta\boldsymbol{\varepsilon}_\theta(t_i)\right]dV+\int_V\mathbf{B}^T\cdot\boldsymbol{\sigma}^C(t_i)dV\right\} \tag{14}$$

$$\Delta\boldsymbol{\rho}=\mathbf{D}\cdot\mathbf{B}\cdot\Delta\mathbf{u}-\lambda^{(k)}\sum_{i=1}^{NV}\Delta\boldsymbol{\sigma}^E(t_i)-\lambda^{(k)}\mathbf{D}\cdot\sum_{i=1}^{NV}\Delta\boldsymbol{\varepsilon}_\theta(t_i)-\sum_{i=1}^{NV}\boldsymbol{\sigma}^C(t_i) \tag{15}$$

$$\boldsymbol{\rho}_0^{(m+1)}=\boldsymbol{\rho}_0^{(m)}+\Delta\boldsymbol{\rho}_0^{(m+1)},\qquad\text{where}\quad\Delta\boldsymbol{\rho}_0^{(m+1)}=\frac{1}{NV}\Delta\boldsymbol{\rho}^{(m+1)} \tag{16}$$

(5) Check the convergence of the dimensionless parameter ξ for all Gauss points using

$$\left|\xi^{(m+1)}(t_i)-\xi^{(m)}(t_i)\right|\le tol1 \tag{17}$$

where $tol1$ is tolerance limit parameter. If ξ is convergent the execution step continues, which means the completion of an inner loop, otherwise the procedure returns to Step (2).

(6) Calculate the maximum value of the dimensionless parameter $\xi^{(m+1)}(t_i)$, i.e.

$$\xi_{\max}^{(k+1)}=\max\left(\xi^{(m+1)}(t_i)\right) \tag{18}$$

(7) Examine the convergence rate

$$\frac{\xi_{\max}^{(k+1)}}{\xi_{\max}^{(k)}}\le tol2,\text{ and }\omega>0.1 \tag{19}$$

where ω is a control parameter. If Condition (19) is satisfied, the load multiplier $\lambda^{(k)}$ is modified by

$$\lambda^{(k+1)}=\frac{\lambda^{(k)}\left(1-\frac{\omega}{2}\cdot\xi_{\max}^{(k+1)}\right)}{\left(1-\omega\cdot\xi_{\max}^{(k+1)}\right)} \tag{20}$$

and ω is halved $\omega=\omega/2$. Otherwise, the load multiplier $\lambda^{(k+1)}$ is updated by

$$\lambda^{(k+1)}=\lambda^{(k)}\left(1-\omega\cdot\xi_{\max}^{(k+1)}\right) \tag{21}$$

(8) Check whether $\xi_{\max}^{(k+1)}$ vanishes within a desired tolerance $tol3$.

$$\xi_{\max}^{(k+1)}\le tol3 \tag{22}$$

(9) Repeat Steps 2–8 till Condition (22) holds. The shakedown limit multiplier λ_{sh} is determined as

$$\lambda_{sh} = \lambda^{(k+1)} \tag{23}$$

The flowchart of the SCM for shakedown analysis is shown in Fig. 2. The iteration control scheme presented allows the numerical procedure to generate a series of decreasing load multipliers, and if the tolerance parameters are appropriately adopted the load multipliers will approach smoothly to the shakedown limit multiplier. The value of $tol1$ in Eq. (17) used to stop the inner loop can influence the accuracy and efficiency of the method. Given that the accuracy of shakedown limit multiplier depends on the final solution of the residual stress and has little relationship to the intermediate solutions, the dynamically changed values of $tol1$ are used here to balance the accuracy and efficiency of the method. The update of load multiplier via Eq. (21) cannot strictly prevent the load multipliers from overshooting below the target value of shakedown limit multiplier. To address this problem, the numerical strategy via (19)–(21) is followed. Although the overshooting might happen in extreme cases, the value is small enough to be negligible. When Condition (19) is satisfied, the load multiplier is adjusted to a value above the shakedown limit multiplier and the process goes on. Thus, the presented method generates a series of decreasing load multiplier approaching to the actual shakedown limit multiplier from above. Because Melan's static shakedown theorem is adopted and when the procedure ends all conditions of this theorem are satisfied, the shakedown limit multiplier calculated is a lower bound solution within the predefined tolerance $tol3$.

3 Numerical Examples and Engineering Applications

The SCM has the significant advantage that it can be incorporated into commercial FE software so that users can establish FE models conveniently. The numerical procedure is implemented into Abaqus platform via user subroutines in this work. The SCM is applied to solve numerous numerical examples. In all examples presented, the materials are assumed homogeneous, isotropic and elastic-perfectly plastic and obey von Mises yield criterion. It is noted that the limit analysis is a special case of shakedown analysis of only one load vertex. All calculations are performed on the computer with 16 GB RAM and Intel Core i7 at 3.39 GHz.

3.1 Square Plate with a Central Circular Hole

The first example is a square plate with a central circular hole under a combination of biaxial mechanical loads and thermal load [18]. Figure 3 displays the structural geometry of $d/L = 0.05$, $D/L = 0.2$ and the quarter FE model. The mesh discretization consists of 432 elements (Abaqus CPS8) with 3×3 Gauss points. The material properties of the structure are listed in Table 1.

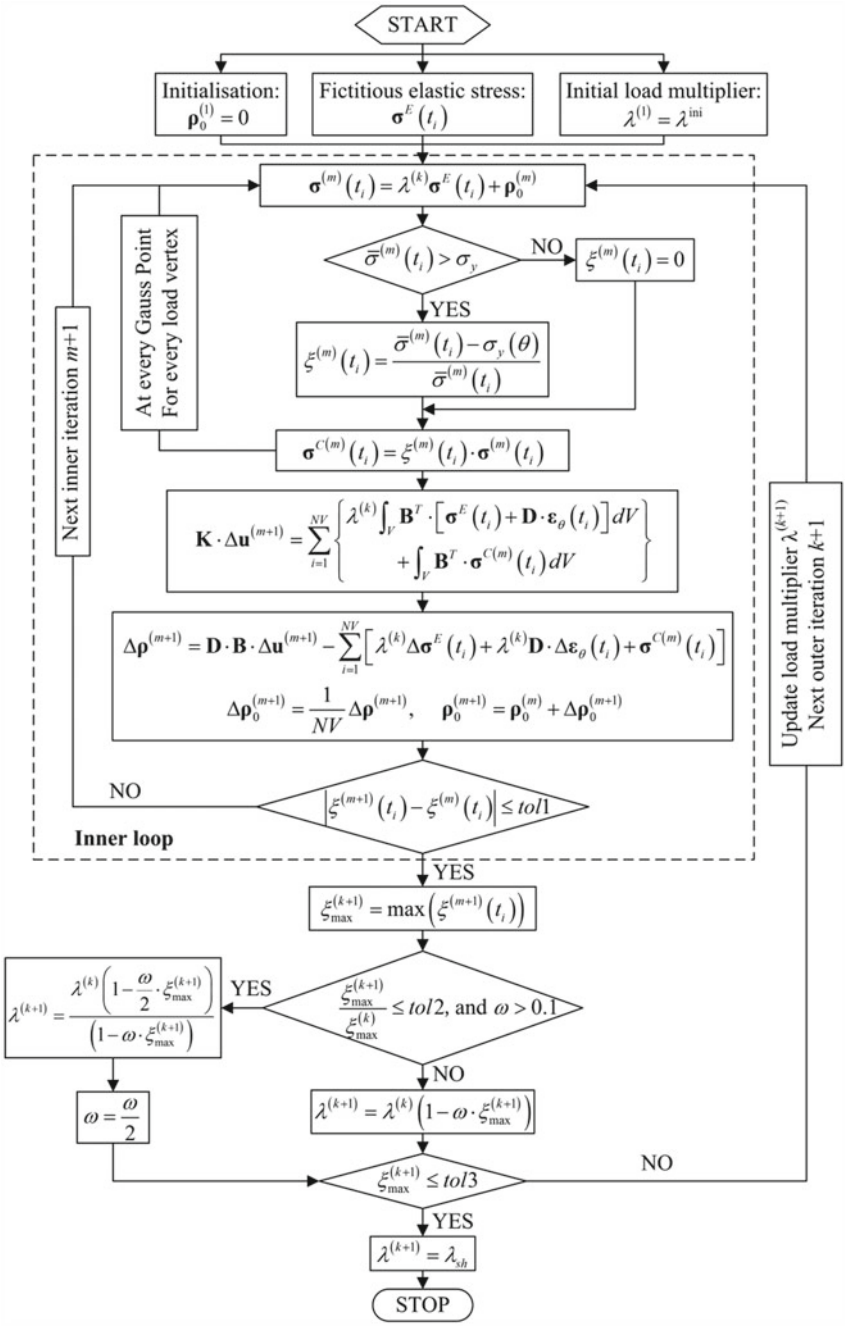

Fig. 2 Flowchart of the SCM for shakedown analysis [21]

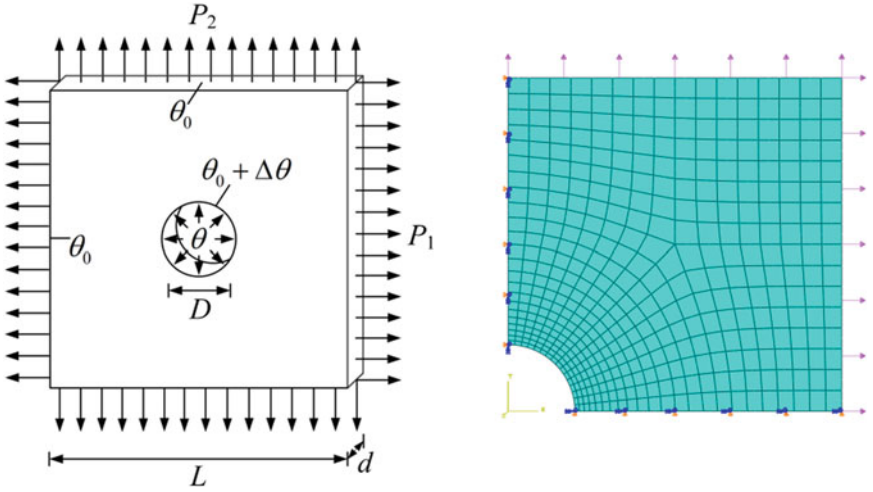

Fig. 3 Geometry of the holed plate and its quarter FE model

Table 1 Material properties of the square plate with a central circular hole

Young's modules E (GPa)	Poisson's ratio v	Yield stress σ_y (MPa)	Coefficient of thermal expansion α ($^\circ C^{-1}$)
208	0.3	360	5×10^{-5}

The holed plate is subjected to three loads, including two uniform normal tractions, P_1 and P_2, and a temperature difference, $\Delta\theta(t)$,

$$\theta = \theta_0 + \Delta\theta \frac{\ln(5D/2r)}{\ln(5)} \tag{24}$$

The base loads are selected as $P_1^* = P_2^* = 360\,\text{MPa}$, $\theta_0 = 0$, and $\Delta\theta^* = 90.2$ °C. The maximum von Mises stress of the holed plate under the base thermal load is σ_θ. Three loading cases are considered here.

(1) Case I

The three loads vary independently in their own ranges.

$$\begin{aligned} 0 \le P_1 &\le \mu_1 P_1^* \\ 0 \le P_2 &\le \mu_2 P_2^* \\ 0 \le \Delta\theta &\le \mu_3 \Delta\theta^* \end{aligned} \tag{25}$$

(2) Case II

The normal traction, P_2, and the thermal load, $\Delta\theta$, vary independently, but the normal traction, P_1, keeps constant.

$$\begin{aligned} P_1 &= \mu_1 P_1^* \\ 0 \le P_2 &\le \mu_2 P_2^* \\ 0 \le \Delta\theta &\le \mu_3 \Delta\theta^* \end{aligned} \tag{26}$$

(3) Case III

The normal tractions, P_1 and P_2, keep constant, but the thermal load, $\Delta\theta$, varies.

$$\begin{aligned} P_1 &= \mu_1 P_1^* \\ P_2 &= \mu_2 P_2^* \\ 0 \le \Delta\theta &\le \mu_3 \Delta\theta^* \end{aligned} \tag{27}$$

The SCM is applied to calculate the shakedown domains of the plate for the three loading cases. Figure 4a, b and c show the 3D shakedown domains of the plate for cases I, II and III, respectively. In Fig. 4a, 111 computed points plot the shakedown surface, consisting of the planes A-B-C and B-C-D. It is noted that all the shakedown limit points are dominated by alternating plasticity. In Fig. 4b, the shakedown surface consists of the plane B-C-D-E and surface A-B-E. It is noted that the points in the plane B-C-D-E are dominated by alternating plasticity whilst the points in the surface A-B-E are dominated by ratcheting. In Fig. 4c, the shakedown surface consists of the surfaces A-B-E-D, B-C-F-E and the plane D-E-F-G. It is noted that the points in the plane D-E-F-G are dominated by alternating plasticity whilst the points in the surfaces A-B-E-D and B-C-F-E are dominated by ratcheting.

To verify the correctness of the calculated results, the SBS incremental elastic-plastic calculations are performed for several specified load points that are depicted as the red, black and blue markers with letters M, N and P in Fig. 4b and c. It should be noted that, in both Fig. 4b and c, the load points M, N, P are located in shakedown region, alternating plasticity region and ratcheting region, respectively. As results, for the load points M, N and P (Fig. 4b), the effective plastic strain histories of a Gauss point over the first 15 load cycles are displayed in Fig. 5. And for the load points M, N and P (Fig. 4c), the effective plastic strain histories of a Gauss point over the first 30 load cycles are displayed in Fig. 6. It can be seen clearly from Fig. 5 and Fig. 6 that the effective plastic strain histories for load points M, N and P exhibit the shakedown, alternating plasticity and ratcheting behavior, respectively. These SBS incremental elastic-plastic analyses reveal the different failure mechanisms expected and verify the correctness the results calculated by the SCM.

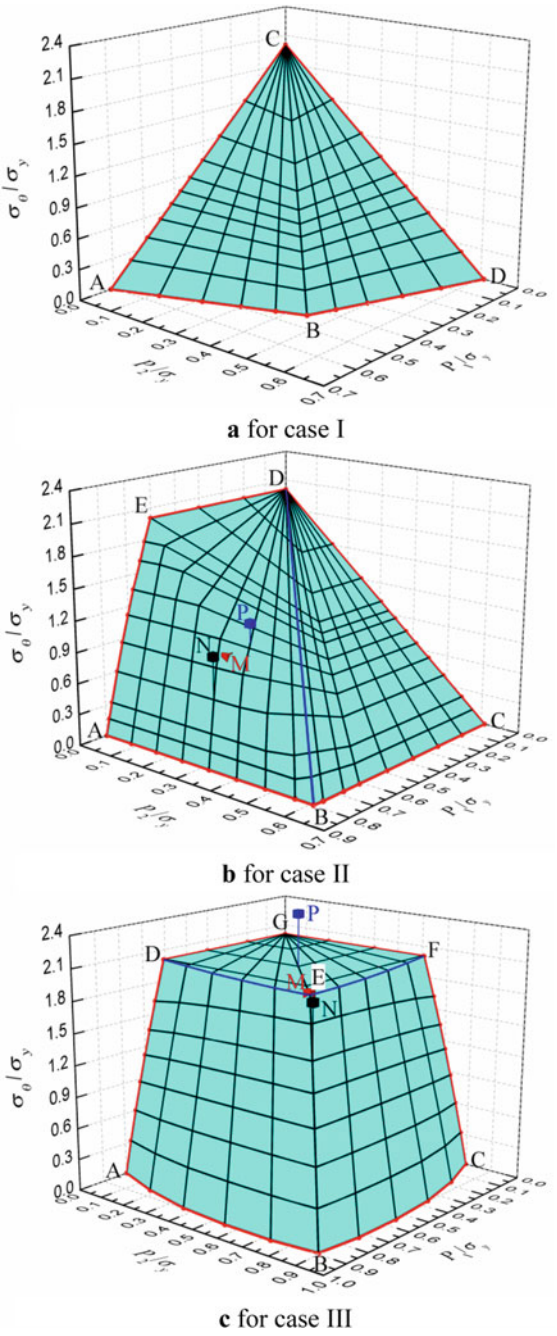

a for case I

b for case II

c for case III

Fig. 4 Shakedown domains of the holed plate in 3D loading space

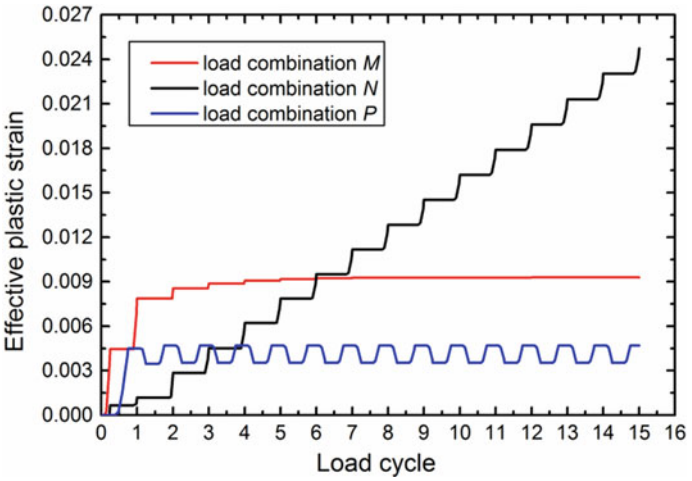

Fig. 5 Effective plastic strains over the first 15 load cycles at a Gauss point of the holed plate from load combinations M, N and P for case II

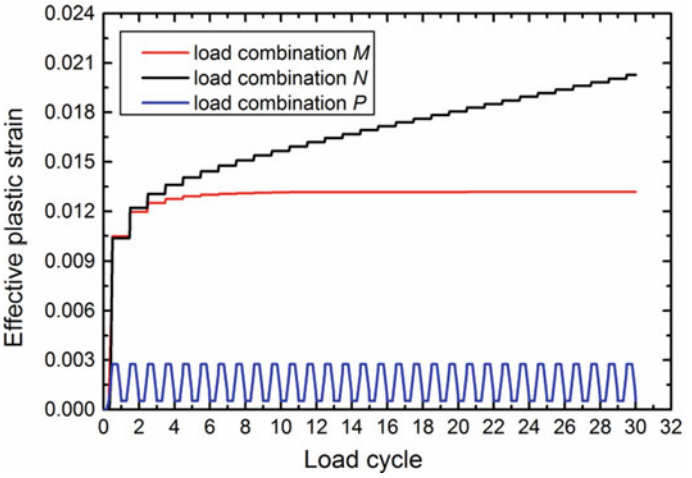

Fig. 6 Effective plastic strains over the first 30 load cycles at a Gauss point of the holed plate from load combinations M, N and P for case III

3.2 Header Component

The second example is a header component from power plant engineering. As shown in Fig. 7, the header component includes a main pipe and two vertical branch pipes with same geometric dimensions. The mesh discretization consists of 27,540 elements (Abaqus C3D20R) and 139,251 nodes, as shown in Fig. 8. The material

properties are listed in Table 2. In the cooling and reheating process, the header component bears complicated load conditions because of the mutual effects with the rest parts of piping system.

Two clusters of loads are applied to the header component, whose base loads are listed in Table 3. For the first load cluster, the internal pressure, P_i, is applied to inner surfaces, and additional tensions caused by the internal pressure are applied to the ends of main and branch pipes. For the second load cluster, the bending moments,

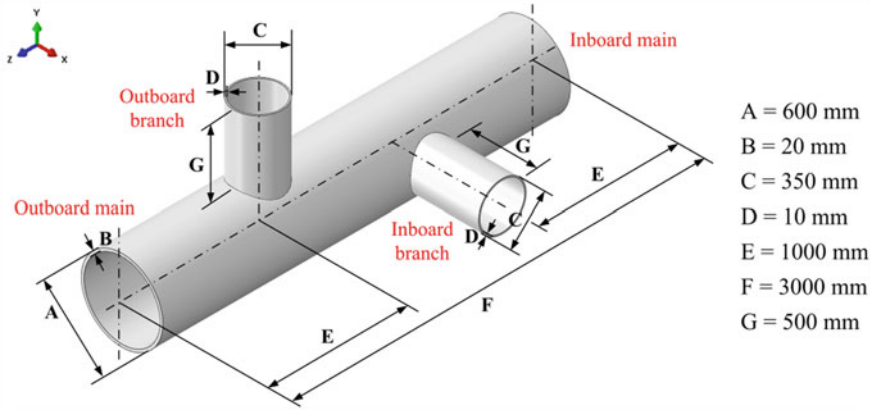

Fig. 7 Geometry of the header component

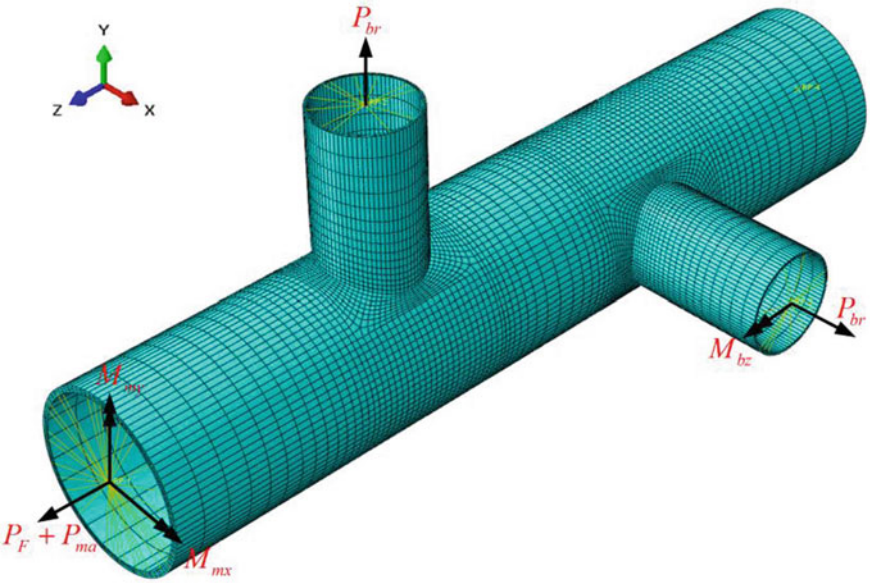

Fig. 8 FE model of the header component

Table 2 Material properties of the header component

Young's modules E (GPa)	Poisson's ratio v	Yield stress σ_y (MPa)
200	0.3	165

M_{mx} and M_{my}, are applied to the outboard main pipe end, and the bending moment M_{bz} is applied to the inboard branch pipe end. It is noted that three bending moments vary simultaneously. Hence, the amplitudes of two clusters of loads are determined by two dimensionless factors, P_0, and M_0. The loading cases of interest are displayed in Fig. 9.

The SCM is applied to calculate the shakedown limits of the header component for the four loading cases. As results, four corresponding shakedown boundaries are presented in Fig. 10. For the loading cases a and b, the shakedown boundaries are all dominated by alternating plasticity whilst for the loading cases c and d, the shakedown boundaries (curve 1 and curve 4 in Fig. 10) are dominated by alternating plasticity and the shakedown boundaries (curve 2 and curve 3 in Fig. 10) are dominated by ratcheting. It is noted that the loading case b is proportional loading. Thus, the

Table 3 Base loads applied to the header component

Load	P_0			M_0		
	Internal pressure P_i (MPa)	Main tension P_{ma} (MPa)	Branch tension P_{br} (MPa)	M_{mx} (kN m)	M_{my} (kN m)	M_{bz} (kN m)
Value	3.64	−24.60	−29.15	240	−160	−9.6

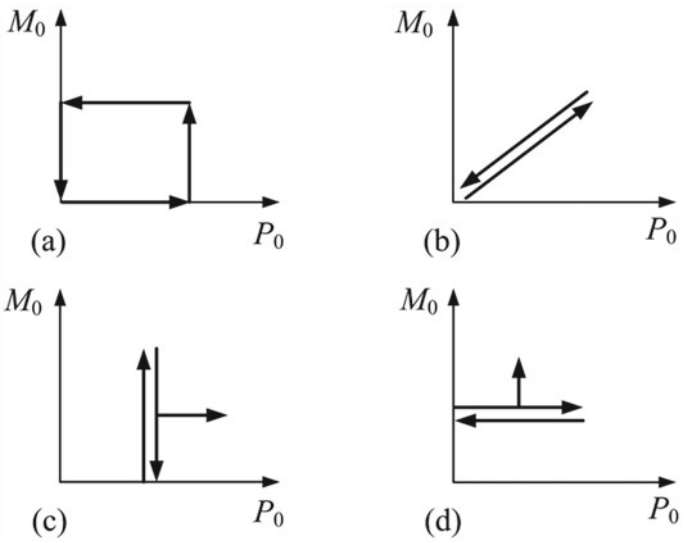

Fig. 9 Four loading cases of interest

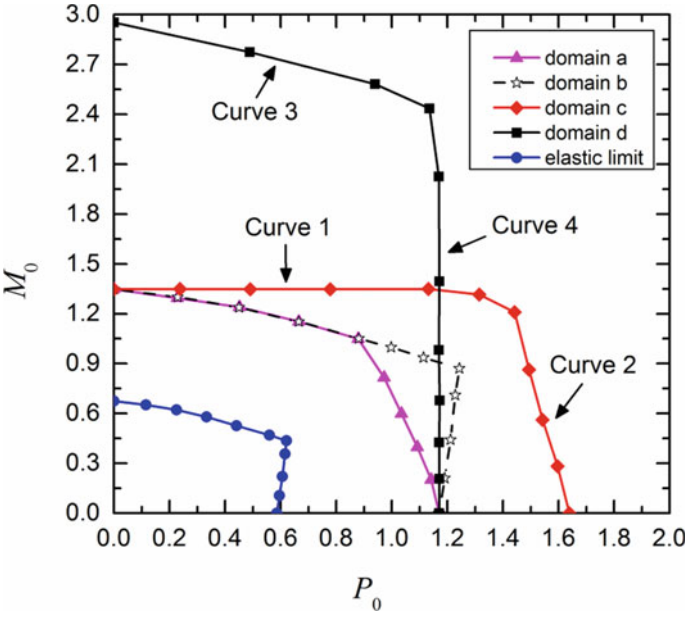

Fig. 10 Shakedown domains of the header component: P_0 versus M_0

shakedown limit will be the lower one between the plastic limit load and the twice of elastic limit load. As a comparison, the elastic boundary is also plotted in Fig. 10. The shakedown boundary curve for the loading case b coincides well with the curve decided by the twice of elastic limit load.

To the authors' knowledge from literature reported, it is the first to show the solution of the shakedown problem with comparable degrees of freedom of FE model [17]. The SCM iterative procedure for shakedown analysis presents good convergence. The CPU time required to complete a calculation does not exceed 40 min using this personal computer. The equivalent residual stress field constructed for static shakedown for the header component is shown in Fig. 11.

3.3 Pipe with an Oblique Nozzle

The third example is a pipe with an oblique nozzle considering the temperature-dependent yield stress. Figure 12 displays the geometry of the structure. This component is subjected to high temperature and internal pressure. When equipment starts up or shuts down, the component bears large temperature variation, and the material properties vary with temperature. Figure 13 displays the FE model that consists of 3,170 elements and 16,928 nodes.

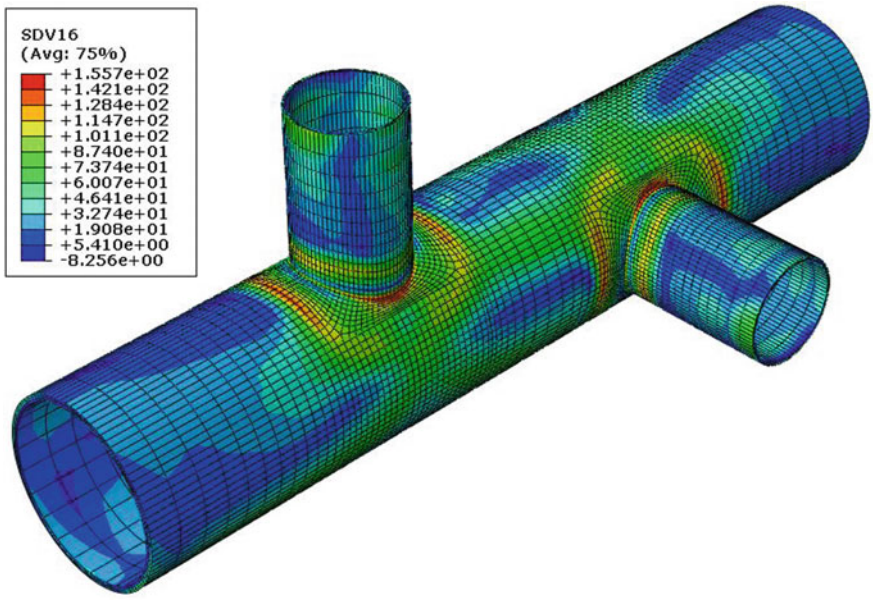

Fig. 11 The equivalent residual stress field constructed for static shakedown for the header component

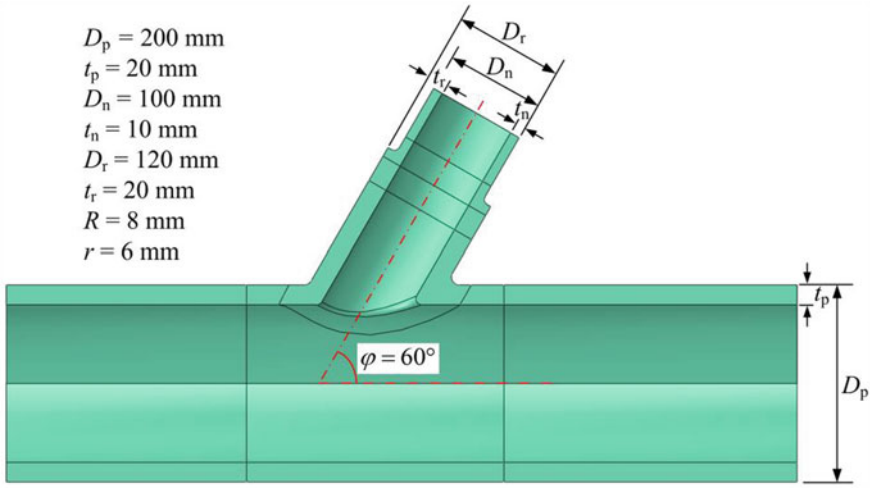

Fig. 12 Geometry of the pipe with oblique nozzle

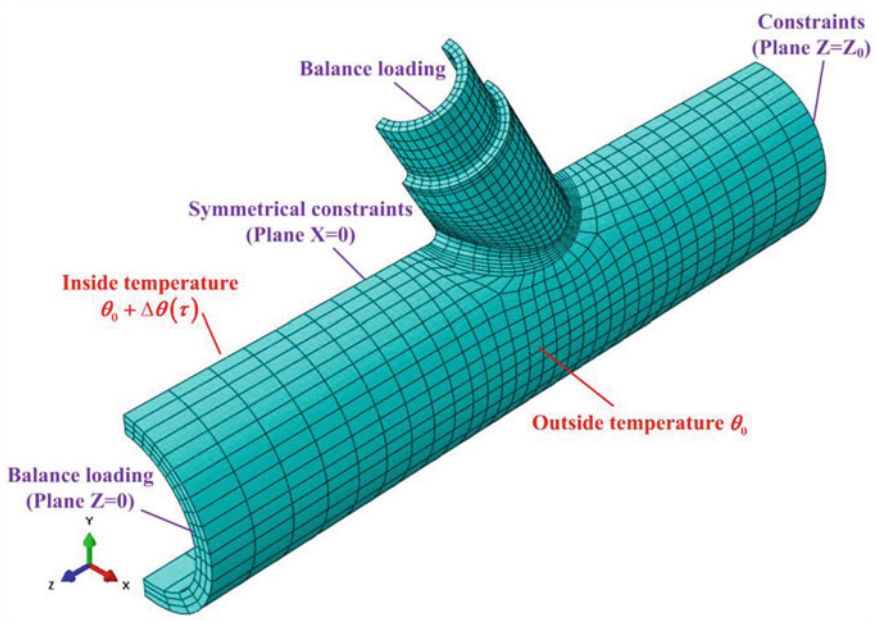

Fig. 13 FE model of the pipe with oblique nozzle

Outside air keeps constant temperature θ_0 and the temperature of inside fluid follows the curve in Fig. 14, which is expressed as $\theta(t) = \theta_0 + \Delta\theta(t)$. The initial temperature of structure and the environment temperature are both $\theta_0 = 20$ °C. The base pressure is $P_0 = 16.5$ MPa. Some material parameters are listed in Table 4. The temperature-dependent yield stress is as follow:

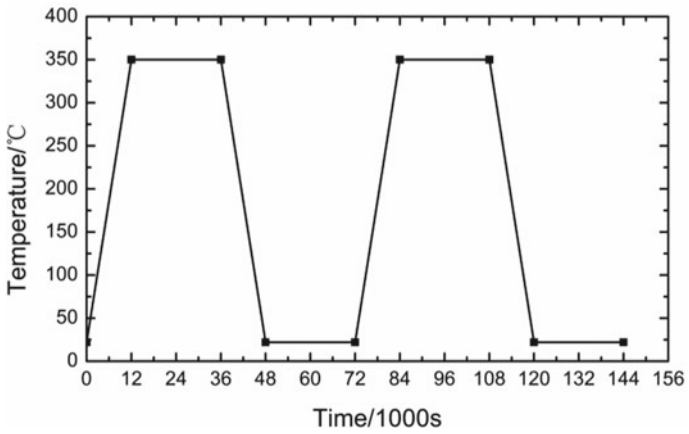

Fig. 14 Temperature history of the inside fluid

Table 4 Material parameters of the pipe with oblique nozzle

Parameters	Value
Thermal expansion coefficient α	2.0×10^{-5}
Thermal conductivity k (W/(m °C))	20
Specific heat capacity c (J/(kg·°C))	440
Transfer coefficient pipe-air h_1 (W/(m^2·°C))	300
Transfer coefficient pipe-fluid h_2 (W/(m^2·°C))	800
Density ρ (kg/m^3)	7800
Yield stress σ_y (MPa)	240
Young's modulus E (MPa)	2.1×10^5
Poisson's ratio v	0.3

$$\sigma_y(\theta) = \sigma_{y_0} + 3 \text{ MPa} - 0.15 \text{ MPa}/^\circ\text{C} \times \theta \tag{28}$$

First, the temperature history is calculated via a transient heat transfer analysis. Then, the thermal elastic stress history is calculated based on the obtained temperature via the structural stress analysis. Nodes 5,451 and 6,308 are selected to show the temperature histories of inside and outside surfaces of the structure, as displayed in Fig. 15. It is obvious from Fig. 15 that the structure bears the maximum temperature gradient at $t = 12{,}000$ s, which leads to the maximum thermal elastic stress. Figure 16a and b, display the von Mises stress fields of the pipe under single thermal load and single base pressure, respectively. Figure 17 displays two typical loading cases considered. For loading case I, temperature and internal pressure vary independently. For loading case II, temperature is cyclic but internal pressure keeps constant. The SCM is applied to calculate the shakedown limits of this pipe considering the temperature-dependent yield stress.

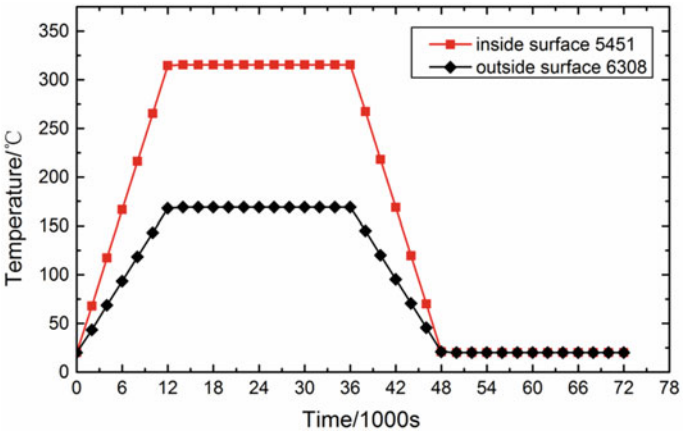

Fig. 15 Temperature histories of node 5451 and node 6308

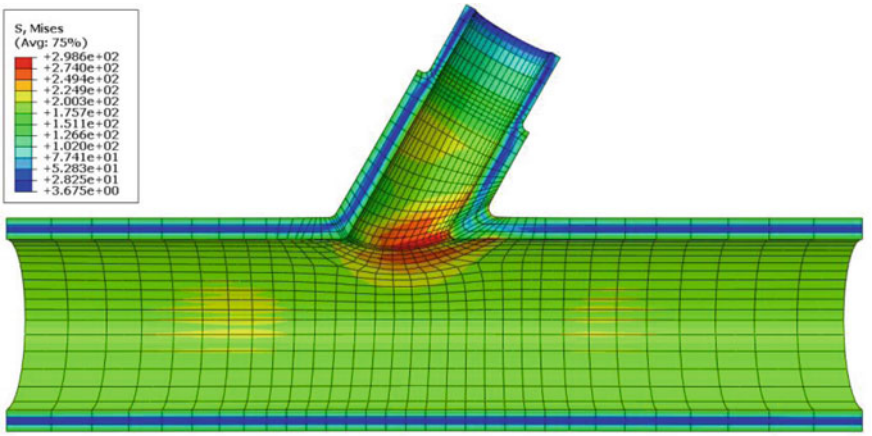

a Thermal stress field at t=12000 s

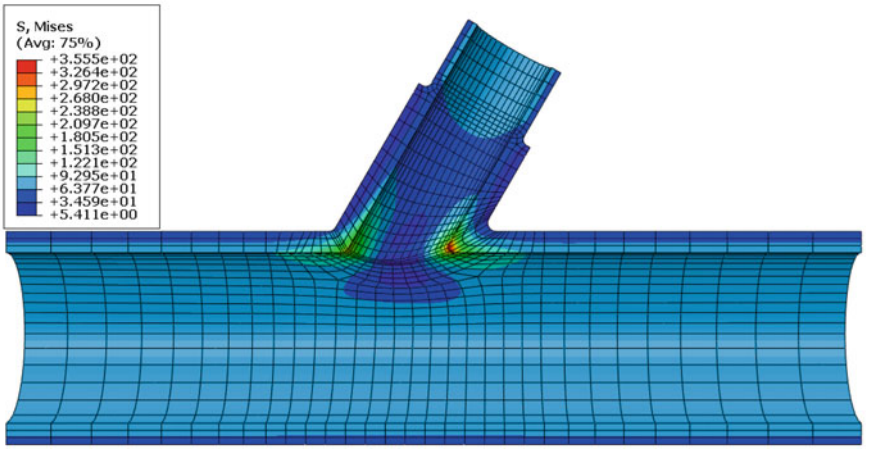

b Mechanical stress field

Fig. 16 Von Mises stress fields of the pipe with oblique nozzle

The shakedown domains of the pipe considering the temperature-dependent and temperature-independent yield stresses for two loading cases are shown in Fig. 18. For loading case I, shakedown boundaries AD and A′D are dominated by alternating plasticity. For loading case II, shakedown boundaries AB and A′B′ are dominated by alternating plasticity but shakedown boundaries BC and B′C are dominated by ratcheting. For both loading cases, shakedown boundaries are narrowed when considering the reduction of yield stress by temperature. It is noted that in regions AB and A′B′, the thermal loading is dominant and the yield stress is largely reduced by high temperature, thus the shakedown limit is significantly decreased.

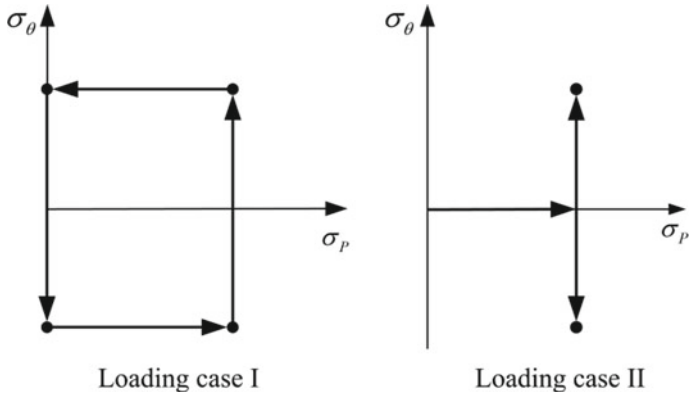

Fig. 17 Two typical loading cases

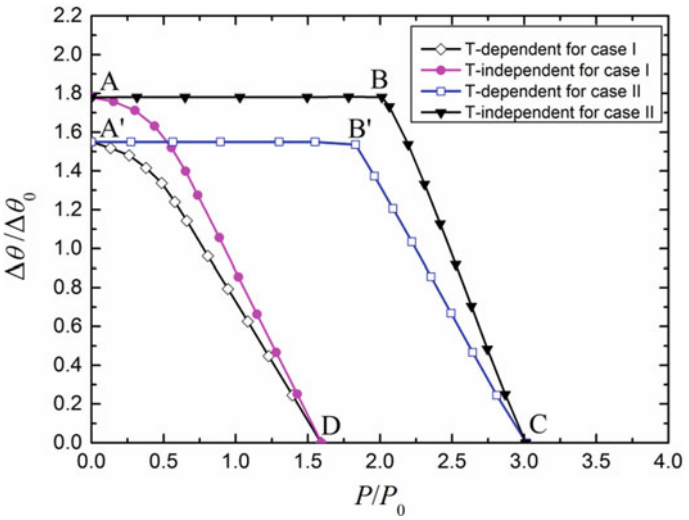

Fig. 18 Shakedown domains of the pipe with oblique nozzle considering temperature-dependent and temperature-independent yield stresses under two loading cases

Figure 19 displays a typical iteration process of load multipliers for shakedown analysis of the pipe with oblique nozzle considering the temperature-dependent yield stress. The horizontal segment indicates the execution of inner loop whilst the leap indicates an update of the load multipliers in the outer loop. The CPU time required for each iteration is about one quarter of that for a complete elastic FE analysis.

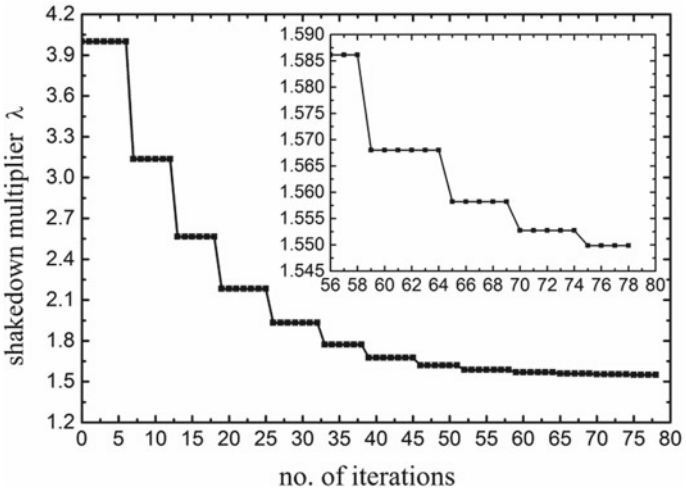

Fig. 19 Typical iteration process of load multipliers for shakedown analysis of the pipe with oblique nozzle considering the temperature-dependent yield stress

3.4 Torispherical Head with a Piping Nozzle

The forth example is a torispherical head with a piping nozzle, whose geometric parameters are shown in Fig. 20 [21–24]. The applied loads include uniform pressure P, axial force F, in-plane bending moment M_{in}, out-of-plane bending moment M_{out}, twisting moment T, and thermal loading defined by a temperature difference $\Delta\theta$. The basic material properties are listed in Table 5.

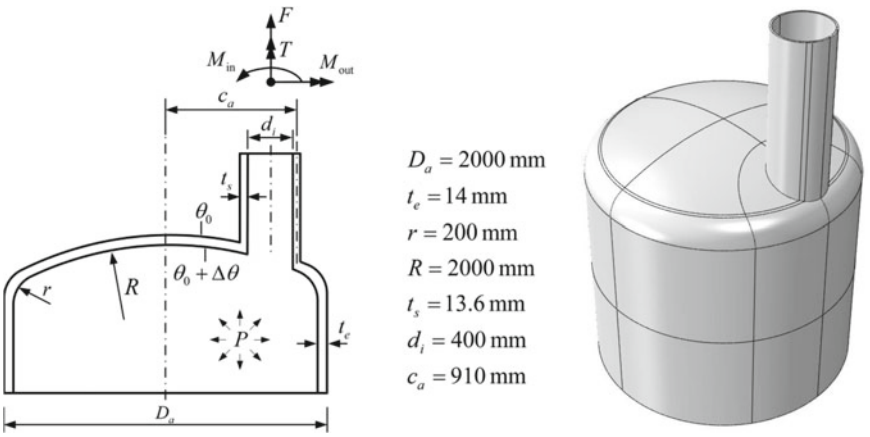

Fig. 20 Geometry of the torispherical head with a piping nozzle

Table 5 Material properties of the torispherical head with a piping nozzle

Yield stress, σ_{y0} (MPa)	340
Young's modulus, E (MPa)	2.0×10^5
Poisson's ratio, v	0.3
Coefficient of thermal expansion, α (/°C)	1.6×10^{-5}
Specific heat capacity, c (J/(kg·°C))	500
Thermal conductivity, k (W/(m·°C))	15
Density, ρ (kg/m^3)	7900

Figure 21 displays the FE model of the torispherical head with a piping nozzle that includes 10,809 elements (Abaqus C3D20R) and 54,804 nodes. To eliminate boundary effects, the lengths of nozzle and of cylindrical shell are about $3d_i$ and D_a, respectively. The cylindrical shell end is restrained in vertical direction but is free in radial direction. It is noted that an additional equivalent axial tension induced by internal pressure is applied to the nozzle end. All nozzle loads are applied to a master node which is coupled to the nozzle end using the Beam-type MPC constraint technique.

The SCM is applied to calculate the plastic limit and shakedown limit loads of the torispherical head with a piping nozzle under various loading conditions, whose results are listed in Table 6. For comparison and verification, the results calculated by the elastic-plastic incremental method within Abaqus are also listed in Table 6. It is noted that the plastic limit load is determined by 15-times elastic slope criterion

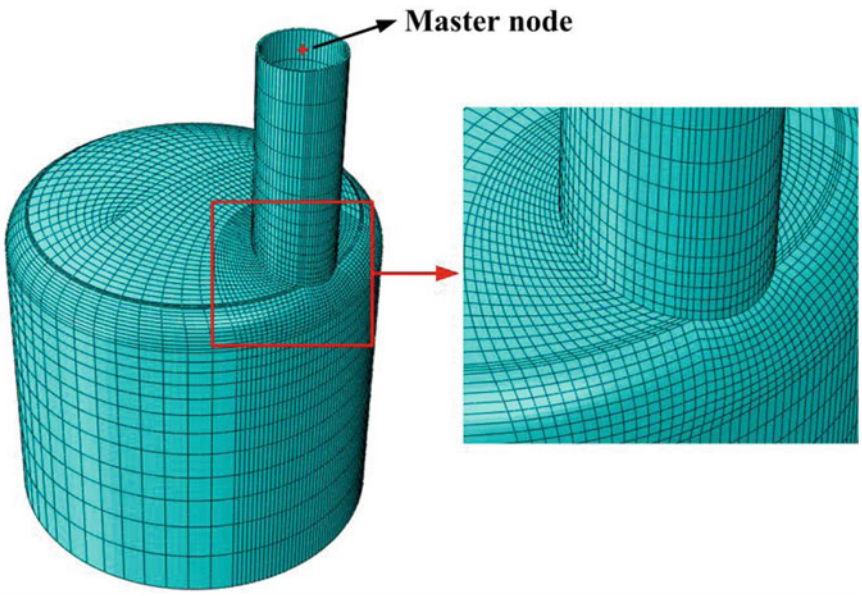

Fig. 21 FE model of the torispherical head with a piping nozzle

Table 6 Shakedown limit and plastic limit loads calculated with two methods

Loading case	SCM		Abaqus	
	Shakedown limit load	Plastic limit load	Double elastic limit load	Plastic limit load
Pressure, P (MPa)	3.004	3.511	3.004	3.523
Axial force, F (kN)	833.8	1451.8	833.9	1463.2
Twisting moment, T (kN m)	364.5	546.4	364.5	551.9
Out-of-plane moment, M_{out} (kN m)	127.9	237.8	127.9	239.2
In-plane moment, M_{in} (kN m)	107.6	248.7	107.7	252.1
Thermal loading, $\Delta\theta$ (°C)	236.0	–	236.0	–

[23] is adopted and the shakedown limit load is determined as the lower one between the plastic limit load and the twice of elastic limit load.

It is evident from Table 6 that the shakedown limit loads calculated with the SCM are very close to the twice of elastic limit loads calculated with Abaqus and are lower than the plastic limit loads. This indicates that these shakedown limit loads are all dominated by alternating plasticity. Furthermore, the good agreement, a maximum relative error of 1.36%, of the plastic limit loads calculated with the SCM and Abaqus shows that the SCM is reliable. It is noted that the thermal loading, causing secondary stress, will not lead to the plastic collapse of structures.

For further comparison, Table 7 gives the comparison of the present solutions [21] with results from literature [22, 23] for different single loads. The present results are approximately in agreement with these reported in [22, 23]. The small difference in value is due to different methods used and different types and sizes of FE meshes selected.

The 3D shakedown domains of the torispherical head with a piping nozzle are investigated. The loading conditions of interest include three independently varying loads, as listed in Table 8. The corresponding loading domain is similar to that displayed in Fig. 1.

As results, four 3D shakedown domains obtained by the SCM are displayed in Figs. 22, 23, 24 and 25. It is noted that the dimensionless loads, normalised by the yield stress σ_{y_0}, are adopted, and more than 100 calculated points are used to depict each of the shakedown boundary surface. In these figures, the red lines represent the

Table 7 Comparison of the present solutions with results from literature

Type	Loading case	Present [21]	Hsieh [23]	Simon [22]
Elastic limit load	Pressure (MPa)	1.502	1.370	1.524
	Axial force (kN)	416.9	450.0	483.1
	In-plane moment (kN m)	53.9	64.7	55.4
	Out-of-plane moment (kN m)	64.0	66.5	–
	Twisting moment (kN m)	182.3	193.8	–
Shakedown limit load	Pressure (MPa)	3.004	–	3.047
	Axial force (kN)	833.8	–	965.9
	In-plane moment (kN m)	107.6	–	110.7
	Out-of-plane moment (kN m)	127.9	–	–
	Twisting moment (kN m)	364.5	–	–
Plastic limit load	Pressure (MPa)	3.511	3.54	–
	Axial force (kN)	1451.8	1630.0	–
	In-plane moment (kN m)	248.7	282.6	–
	Out-of-plane moment (kN m)	237.8	265.8	–
	Twisting moment (kN m)	546.4	625.0	–

Table 8 3D loading domains of interest

Loading condition	Loading domain
P, F, and M_{in}	$0 \le P \le \mu_1^+ P_0,\ 0 \le F \le \mu_2^+ F_0$ and $0 \le M_{\text{in}} \le \mu_3^+ M_{\text{in0}}$
P, F, and M_{out}	$0 \le P \le \mu_1^+ P_0,\ 0 \le F \le \mu_2^+ F_0$ and $0 \le M_{\text{out}} \le \mu_3^+ M_{\text{out0}}$
P, F, and T	$0 \le P \le \mu_1^+ P_0,\ 0 \le F \le \mu_2^+ F_0$ and $0 \le T \le \mu_3^+ T_0$
P, F, and $\Delta\theta$	$0 \le P \le \mu_1^+ P_0,\ 0 \le F \le \mu_2^+ F_0$ and $0 \le \Delta\theta \le \mu_3^+ \Delta\theta_0$

shakedown boundary curves of the structure under specific two-dimensional loading domains.

In above examples, the material properties are independent to temperature (see Table 5). Here a temperature-dependent yield stress $\sigma_y(\theta)$ is considered, which is a linear function of θ, i.e.

$$\sigma_y(\theta) = \sigma_{y_0} - 0.3 \times (\theta - 20\ ^\circ\text{C}) \tag{29}$$

Taking a loading condition as an example, i.e.

$$0 \le P \le \mu_1^+ P_0,\ 0 \le F \le \mu_2^+ F_0 \text{ and } 0 \le \Delta\theta \le \mu_3^+ \Delta\theta_0 \tag{30}$$

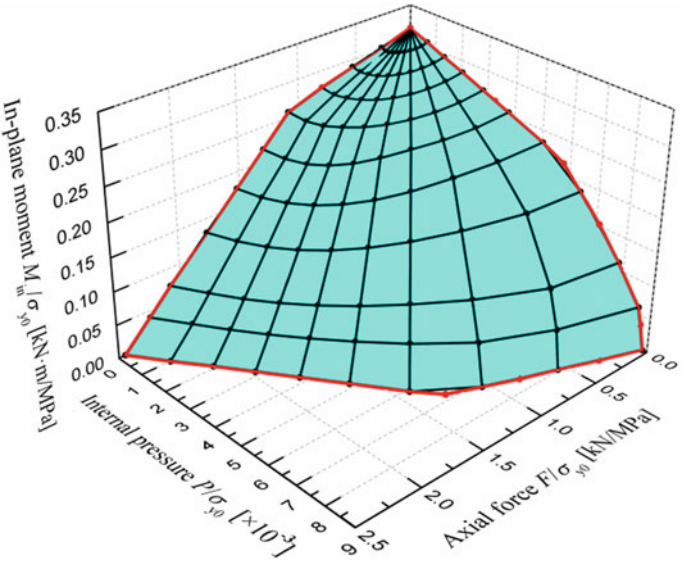

Fig. 22 3D shakedown domain: in-plane bending moment, internal pressure, and axial force

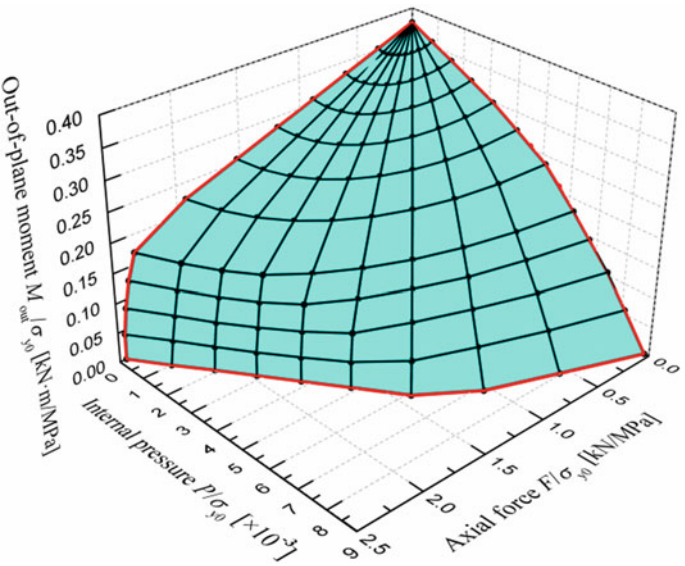

Fig. 23 3D shakedown domain: out-of-plane bending moment, internal pressure, and axial force

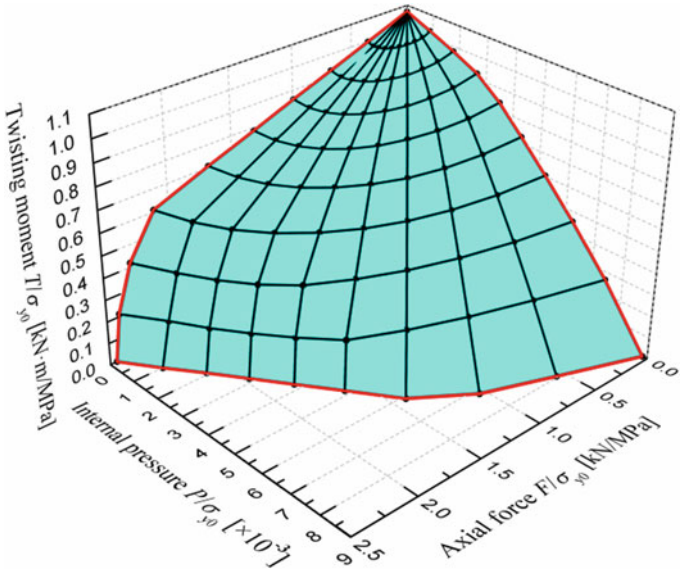

Fig. 24 3D shakedown domain: twisting moment, internal pressure, and axial force

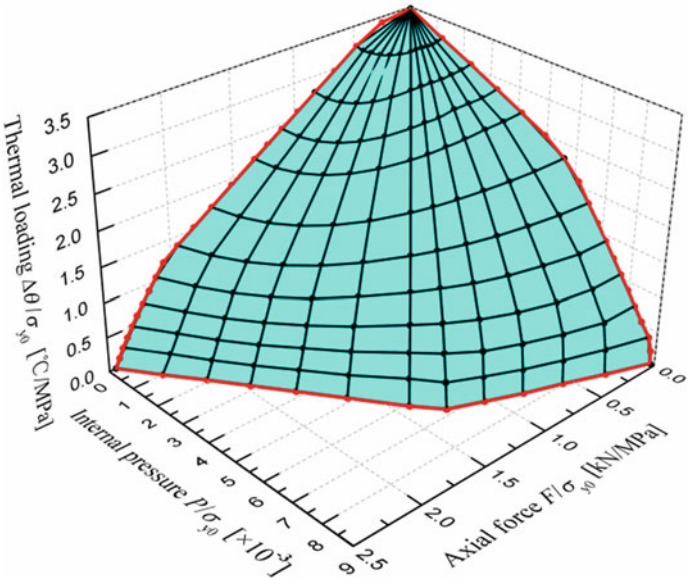

Fig. 25 3D shakedown domain: thermal loading, internal pressure, and axial force

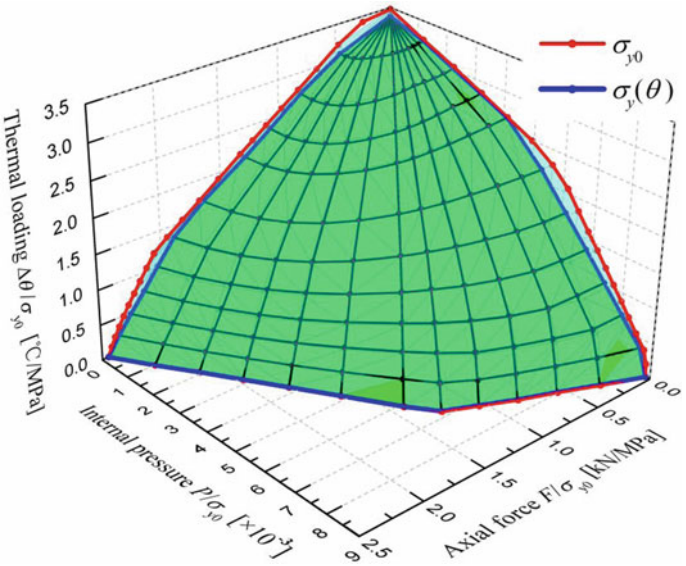

Fig. 26 3D shakedown domains with the temperature-dependent and temperature-independent yield stresses: thermal loading, internal pressure, and axial force

the resulting 3D shakedown domain considering the temperature-dependent yield stress $\sigma_y(\theta)$ is displayed as the green surface in Fig. 26. For comparison, the 3D shakedown domain with a constant yield stress σ_{y0} is displayed in Fig. 26 (the cyan surface) additionally.

Although the same geometric parameters and similar loading conditions with the paper by Simon et al. [22] are used, the completely different shakedown analysis method is employed to demonstrate the performance of the presented SCM in solving large-scale shakedown problem. More complicated loading cases including out-of-plane moment is considered in this paper so that the full geometric model is established while only one-half of the geometric model is adopted in [22]. In addition, this paper investigates the influence of temperature-dependent yield stress on shakedown boundary. In general, when using the mathematical programming method, such as the IPM, to solve shakedown problem, the computing time depends on the number of loads [22, 25]. However, the computing time has little relationship to the loading scenario using the SCM presented in this paper. For a FE model consisting of 10,809 quadratic elements and 54,804 nodes in this numerical example, the CPU time required by the SCM varies from 0.2 h to 0.4 h, while for a FE model consisting of 6,376 linear elements and 9,645 nodes, the computing time by the IPM is less than 10 h [22]. It is evident that the SCM is capable of solving the shakedown problem for large-scale practical engineering structures in reasonable time.

4 Concluding Remarks

In this paper, a recently proposed direct method, SCM, has been introduced to solve the shakedown problem for large-scale practical engineering structures considering the complex loading conditions. In first, the theoretical and numerical aspects of the SCM have been presented. The SCM includes the two-level iterative procedure based on a series of linear FE solutions, instead of using a mathematical programming technique. The inner loop constructs the residual stress field for static shakedown while the outer loop updates load multipliers using an effective and robust iteration control scheme. Then the numerical procedure of the SCM has been implemented into the Abaqus platform, making it become a general utility tool for shakedown analysis of complex structures. Next four numerical examples, including square plate with a central circular hole, header component, pipe with an oblique nozzle, torispherical head with a piping nozzle, have been presented to illustrate the performance of the method. The 3D loading domain and the effect of temperature on yield stress have also been considered. The calculated results have been validated with the SBS elastic-plastic incremental method and results from literature. It has been proven that the SCM is a powerful tool for performing shakedown analysis of large-scale structures under complex multi-loading systems with huge computational advantage, and has application prospects in the structural design and integrity assessment of practical engineering structures. Although the present paper only introduces the application of the method to the elastic-perfectly plastic material, the shakedown analysis with consideration of material hardening has been accomplished and these works will be reported in forthcoming paper.

Acknowledgements The authors gratefully acknowledge the support of the National Science Foundation for Distinguished Young Scholars of China (Grant No. 11325211) and the National Natural Science Foundation of China (Grant No. 11672147).

References

1. Weichert, D., Ponter, A.: A historical view on shakedown theory. In: Stein, E. (ed.) The History of Theoretical, Material and Computational Mechanics-Mathematics Meets Mechanics and Engineering, pp. 169–193. Springer (2014). https://doi.org/10.1007/978-3-642-39905-3_11
2. König, J.A.: Shakedown of Elastic-Plastic Structures. Elsevier, Warszawa, Poland (1987)
3. Makrodimopoulos, A., Martin, C.M.: Lower bound limit analysis of cohesive-frictional materials using second-order cone programming. Int. J. Numer. Meth. Eng. **66**(4), 604–634 (2006). https://doi.org/10.1002/nme.1567
4. Zhang, X.F., Liu, Y.H., Zhao, Y.N., Cen, Z.Z.: Lower bound limit analysis by the symmetric Galerkin boundary element method and the Complex method. Comput. Method Appl. Mech. **191**(17–18), 1967–1982 (2002). https://doi.org/10.1016/s0045-7825(01)00363-2
5. Garcea, G., Leonetti, L.: A unified mathematical programming formulation of strain driven and interior point algorithms for shakedown and limit analysis. Int. J. Numer. Meth. Eng. **88**(11), 1085–1111 (2011). https://doi.org/10.1002/nme.3188
6. Simon, J.W., Weichert, D.: Numerical lower bound shakedown analysis of engineering structures. Comput. Method Appl. Mech. **200**(41–44), 2828–2839 (2011). https://doi.org/10.1016/j.cma.2011.05.006
7. Zhang, Y.: An iteration algorithm for kinematic shakedown analysis. Comput. Method Appl. Mech. **127**(1–4), 217–226 (1995). https://doi.org/10.1016/0045-7825(95)00121-6
8. Liu, Y.H., Cen, Z.Z., Xu, B.Y.: A numerical-method for plastic limit analysis of 3-D structures. Int. J. Solids Struct. **32**(12), 1645–1658 (1995)
9. Zouain, N., Borges, L., Silveira, J.L.: An algorithm for shakedown analysis with nonlinear yield functions. Comput. Method Appl. Mech. **191**(23–24), 2463–2481 (2002). https://doi.org/10.1016/S0045-7825(01)00374-7
10. Mackenzie, D., Shi, J., Boyle, J.T.: Finite-element modeling for limit analysis by the elastic compensation method. Comput. Struct. **51**(4), 403–410 (1994)
11. Ponter, A.R.S., Carter, K.F.: Shakedown state simulation techniques based on linear elastic solutions. Comput. Method Appl. Mech. **140**(3–4), 259–279 (1997). https://doi.org/10.1016/S0045-7825(96)01105-X
12. Chen, H.F., Ponter, A.R.S.: Shakedown and limit analyses for 3-D structures using the linear matching method. Int. J. Press. Vessels Pip. **78**(6), 443–451 (2001). https://doi.org/10.1016/S0308-0161(01)00052-7
13. Chen, H.F., Ponter, A.R.S.: A method for the evaluation of a ratchet limit and the amplitude of plastic strain for bodies subjected to cyclic loading. Eur. J. Mech. A-Solid **20**(4), 555–571 (2001). https://doi.org/10.1016/S0997-7538(01)01162-7
14. Lytwyn, M., Chen, H.F., Ponter, A.R.S.: A generalised method for ratchet analysis of structures undergoing arbitrary thermo-mechanical load histories. Int. J. Numer. Meth. Eng. **104**(2), 104–124 (2015). https://doi.org/10.1002/nme.4924
15. Spiliopoulos, K.V., Panagiotou, K.D.: A residual stress decomposition based method for the shakedown analysis of structures. Comput. Method Appl. Mech. **276**, 410–430 (2014). https://doi.org/10.1016/j.cma.2014.03.019
16. Spiliopoulos, K.V., Panagiotou, K.D.: An enhanced numerical procedure for the shakedown analysis in multidimensional loading domains. Comput. Struct. **193**(Suppl. C), 155–171 (2017). https://doi.org/10.1016/j.compstruc.2017.08.008
17. Peng, H., Liu, Y., Chen, H.: A numerical formulation and algorithm for limit and shakedown analysis of large-scale elastoplastic structures. Comput. Mech. **63**(1), 1–22 (2019). https://doi.org/10.1007/s00466-018-1581-x
18. Peng, H., Liu, Y., Chen, H., Shen, J.: Shakedown analysis of engineering structures under multiple variable mechanical and thermal loads using the stress compensation method. Int. J. Mech. Sci. **140**, 361–375 (2018). https://doi.org/10.1016/j.ijmecsci.2018.03.020
19. Gokhfeld, D.A., Charniavsky, O.F.: Limit Analysis of Structures at Thermal Cycling, vol. 4. Sijthoff & Noordhoff edn. Alphen aan den Rijn, The Netherlands (1980)

20. Borino, G.: Consistent shakedown theorems for materials with temperature dependent yield functions. Int. J. Solids Struct. **37**(22), 3121–3147 (2000). https://doi.org/10.1016/S0020-7683(99)00114-6
21. Peng, H., Shen, J., Liu, Y., Chen, H.: Shakedown analysis of a torispherical head with a piping nozzle under combined loads by the stress compensation method. Int. J. Press. Vessels Pip. **172**, 107–118 (2019). https://doi.org/10.1016/j.ijpvp.2019.03.028
22. Simon, J.W., Chen, G., Weichert, D.: Shakedown analysis of nozzles in the knuckle region of torispherical heads under multiple thermo-mechanical loadings. Int. J. Press. Vessels Pip. **116**, 47–55 (2014). https://doi.org/10.1016/j.ijpvp.2014.01.004
23. Hsieh, M.F., Moffat, D.G., Mistry, J.: Nozzles in the knuckle region of a torispherical head: limit load interaction under combined pressure and piping loads. Int. J. Press. Vessels Pip. **77**(13), 807–815 (2000). https://doi.org/10.1016/S0308-0161(00)00073-9
24. Saal, H., Bauer, H., Häderle, M.-U.: Flexibility factors for nozzles in the knuckle region of dished pressure vessel heads. Int. J. Press. Vessels Pip. **70**(3), 151–160 (1997). https://doi.org/10.1016/S0308-0161(96)00020-8
25. Simon, J.W., Weichert, D.: Shakedown analysis with multidimensional loading spaces. Comput. Mech. **49**(4), 477–485 (2012). https://doi.org/10.1007/s00466-011-0656-8